LETTER

doi:10.1038/nature12322

In vivo cardiac reprogramming contributes to zebrafish heart regeneration

Ruilin Zhang[1], Peidong Han[1], Hongbo Yang[1], Kunfu Ouyang[1], Derek Lee[1], Yi-Fan Lin[2], Karen Ocorr[3], Guson Kang[4], Ju Chen[1], Didier Y. R. Stainier[4]†, Deborah Yelon[2] & Neil C. Chi[1,5]

Despite current treatment regimens, heart failure remains the leading cause of morbidity and mortality in the developed world due to the limited capacity of adult mammalian ventricular cardiomyocytes to divide and replace ventricular myocardium lost from ischaemia-induced infarct[1,2]. Hence there is great interest to identify potential cellular sources and strategies to generate new ventricular myocardium[3]. Past studies have shown that fish and amphibians and early postnatal mammalian ventricular cardiomyocytes can proliferate to help regenerate injured ventricles[4–6]; however, recent studies have suggested that additional endogenous cellular sources may contribute to this overall ventricular regeneration[3]. Here we have developed, in the zebrafish (*Danio rerio*), a combination of fluorescent reporter transgenes, genetic fate-mapping strategies and a ventricle-specific genetic ablation system to discover that differentiated atrial cardiomyocytes can transdifferentiate into ventricular cardiomyocytes to contribute to zebrafish cardiac ventricular regeneration. Using *in vivo* time-lapse and confocal imaging, we monitored the dynamic cellular events during atrial-to-ventricular cardiomyocyte transdifferentiation to define intermediate cardiac reprogramming stages. We observed that Notch signalling becomes activated in the atrial endocardium following ventricular ablation, and discovered that inhibiting Notch signalling blocked the atrial-to-ventricular transdifferentiation and cardiac regeneration. Overall, these studies not only provide evidence for the plasticity of cardiac lineages during myocardial injury, but more importantly reveal an abundant new potential cardiac resident cellular source for cardiac ventricular regeneration.

Atrial cardiomyocytes appear to have the remarkable capacity to divide in many adult vertebrate hearts including mammals during cardiac ventricular injury[7,8]; however, the role of these proliferating atrial cardiomyocytes remains unclear. To address this issue, we have generated in the zebrafish, a genetic cardiac ventricle-specific nitroreductase (NTR)-mediated ablation system[9], *Tg*(*vmhc:mCherry–NTR*)^{s957}, using the *ventricular myosin heavy chain* (*vmhc*) promoter[10]. Thus, this ablation system permits the targeted destruction of ventricular cardiomyocytes after metronidazole (MTZ) treatment (Fig. 1). To track both atrial and ventricular cardiomyocytes during ventricular injury, we fused the mCherry fluorescent protein to NTR to label ventricular cardiomyocytes in red (venCherry), as well as using the *atrial myosin heavy chain* (*amhc*) promoter to create the *Tg*(*amhc:eGFP*)^{s958} transgenic line, which marks with enhanced green fluorescent protein the atrial cardiomyocytes (atrGFP). As a result, we observed that the expression of mCherry and GFP in these reporter lines were restricted to ventricular and atrial cardiomyocytes, respectively, throughout development (Supplementary Fig. 1a–d). In order to visually monitor *in vivo* the dynamic cellular events that transpire throughout ventricular injury and regeneration within the same animal, the ventricles of *Tg*(*vmhc:mCherry–NTR*); *Tg*(*amhc:eGFP*) hearts were ablated at 3–4 days post-fertilization (dpf), an age when the zebrafish heart has completed cardiac looping and cardiac chamber cardiomyocytes have fully differentiated[11], but the zebrafish remains optically clear. As a result, 4 dpf ablated *vmhc:mCherry–NTR* ventricles displayed statistically significant reduction in venCherry fluorescence by 24 h post MTZ treatment (hours post treatment, hpt) (Fig. 1b, Supplementary Fig. 2a). This rapid decrease in venCherry fluorescence was accompanied by a reduction in ventricular size (Fig. 1b, Supplementary Fig. 2b) and function (fractional area change decreased from 42% to 16% at 24 hpt, $n = 5$, $P = 0.004$; Supplementary Videos 1 and 2; Supplementary Fig. 3a–c), leading to pericardial oedema and overall decreased blood circulation. TUNEL (TdT-mediated dUTP nick end labelling) cell-death assays revealed that this decrease in ventricular function and size was due to an increase in ventricular cardiomyocyte death (Fig. 1f). Conversely, we observed that the atria significantly enlarged (Supplementary Fig. 2b) and maintained normal contractile function (Supplementary Fig. 3d) during this reduction in ventricular size and function.

By 48 hpt, we observed in these injured ventricles an accretion of new venCherry^{+} cardiomyocytes adjacent to the atrioventricular canal (AVC) (Fig. 1c, asterisk), which continued to expand across the ventricle over the next 48 h to restore lost ventricular myocardium nearest

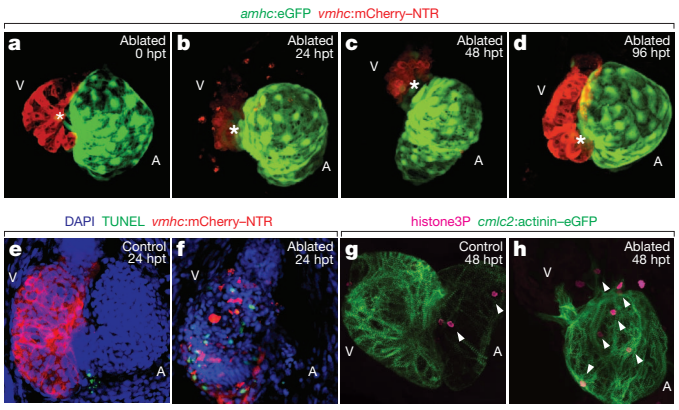

Figure 1 | Genetic ventricular-specific cardiomyocyte ablation results in ventricular cardiomyocyte death and subsequent regeneration. **a**–**d**, Metronidazole (MTZ)-ablated *Tg*(*vmhc:mCherry–NTR*; *amhc:eGFP*) ventricular cardiomyocytes at 0 h (**a**), 24 h (**b**), 48 h (**c**) and 96 h (**d**) post-treatment (hpt). Ventricular cardiomyocytes (red), atrial cardiomyocytes (green), AVC (asterisks). **e**, **f**, TUNEL staining (green) in 24 hpt *Tg*(*vmhc:mCherry–NTR*) control (**e**) and ablated (**f**) ventricles (red) at 4 dpf. DAPI (4′,6-diamidino-2-phenylindole), blue. **g**, **h**, Anti-phospho-histone H3 staining (magenta) in 48 hpt *Tg*(*vmhc:mCherry–NTR*; *cmlc2:actinin–eGFP*) control (**g**) and ablated (**h**) hearts (green) at 5 dpf. Arrowheads indicate anti-phospho-histone H3 positive cells. A, atrium; V, ventricle. Magnification, ×40 objective.

[1]Department of Medicine, Division of Cardiology, University of California, San Diego, La Jolla, California 92093, USA. [2]Division of Biological Sciences, University of California, San Diego, La Jolla, California 92093, USA. [3]Development and Aging Program, Sanford-Burnham Institute for Medical Research, La Jolla, California 92037, USA. [4]Department of Biochemistry and Biophysics, University of California, San Francisco, San Francisco, California 94158, USA. [5]Institute of Genomic Medicine, University of California, San Diego, La Jolla, California 92093, USA. †Present address: Department of Developmental Genetics, Max Planck Institute for Heart and Lung Research, Ludwigstrasse 43, 61231 Bad Nauheim, Germany.

the AVC by 96 hpt (Fig. 1d, asterisk). Subsequently, ventricular cardiac function recovered in these injured hearts to nearly that of age-matched controls by 96 hpt (fractional area change of ablated and control ventricle was 38% and 39%, respectively; $n = 5$, $P = 0.49$; Supplementary Fig. 3c), allowing for survival of these ventricle-ablated fish into adulthood. Anti-phospho-histone H3 immunostaining revealed that ventricular injury resulted in not only ventricular but also atrial cardiomyocyte proliferation (Fig. 1g, h; Supplementary Fig. 4), as observed in other cardiac injury and regeneration models[4,6,12]. Although this cardiomyocyte cell division peaked by 48 hpt in both cardiac chambers (Supplementary Fig. 4d, e), there was a particularly significant atrial cardiomyocyte proliferative increase that remained elevated up to 84 hpt.

During the ventricular recovery, we observed the presence of low expressing atrGFP cardiomyocytes (atrGFP^{lo}) within the injured ventricle near the AVC between 24–48 hpt (Fig. 1b, c and 2b), whereas atrGFP cardiomyocytes were never observed in the ventricle of control hearts (Fig. 2a). Optical sections of the AVC region revealed that these atrGFP^{lo} cardiomyocytes co-expressed the venCherry marker in the ablated ventricles (Fig. 2b, right panel, arrowheads), but were not detected in unablated ventricles (Fig. 2a, right panel). To further confirm these findings, we examined the gene expression of *amhc* and *vmhc* in the hearts of these ablated ventricles and observed that *amhc* was expressed throughout the atrium and frequently in the ventricle at the AVC by 24–48 hpt, where we observed the double-labelled

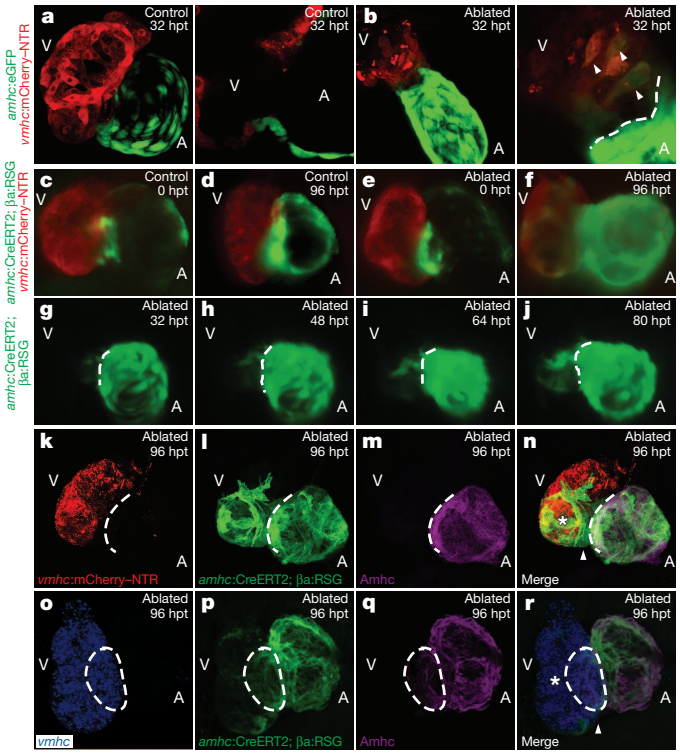

Figure 2 | *In vivo* cardiac reprogramming contributes to zebrafish ventricular regeneration. **a**, **b**, 32 hpt *Tg*(*vmhc:mCherry–NTR*; *amhc:eGFP*) control (**a**) and ablated (**b**) hearts. The AVC section of **a** and **b** are shown in the respective right images of these panels. Arrowheads indicate mCherry^{+} GFP^{+} cardiomyocytes. **c**–**j**, 4-HT-treated *Tg*(*vmhc:mCherry–NTR*; *amhc:CreERT2*; *β-actin2:RSG*) zebrafish in control (**c**, **d**) or ablated (**e**–**j**) hearts at 0 hpt (**c**, **e**), 32 hpt (**g**), 48 hpt (**h**), 64 hpt (**i**), 80 hpt (**j**) and 96 hpt (**d**, **f**). **g**–**j**, 32–80 hpt GFP time-lapse imaging. **k**–**r**, 4-HT-treated *Tg*(*vmhc:mCherry–NTR*; *amhc:CreERT2*; *β-actin2:RSG*) ablated hearts at 96 hpt; venCherry^{+} (red) (**k**); cre-atrGFP^{+} (green) (**l**, **p**); anti-Amhc (S46) (magenta) (**m**, **q**); merge (**n**, **r**) and *vmhc* RNA (blue) (**o**). Asterisk indicates venCherry^{+} cre-atrGFP^{+} Amhc^{-} (**n**) or *vmhc*$^{+}$ cre-atrGFP^{+} Amhc^{-} (**r**) ventricular cardiomyocytes. Arrowhead indicates venCherry^{-} cre-atrGFP^{+} Ahmc^{-} (**n**) or *vmhc*$^{-}$ cre-atrGFP^{+} Amhc^{-} (**r**) ventricular cardiomyocytes. A, atrium; V, ventricle; dashed lines indicate the atrioventricular boundary.

atrGFP^{lo} venCherry^{+} cardiomyocytes; whereas *vmhc* was expressed throughout the ventricle, but rarely in the atrium and only at 12–24 hpt. (Supplementary Fig. 5). Thus, these findings indicate that during injury, pre-existing atrial cardiomyocytes may migrate to the ventricle to transdifferentiate into ventricular cardiomyocytes, or alternatively, proliferating dedifferentiated ventricular cardiomyocytes may need to activate an atrial program before fully differentiating into ventricular cardiomyocytes. Given that we still observe some proliferating pre-existing venCherry cardiomyocytes that never express the atrGFP marker, we speculate that the atrial-to-ventricular cardiomyocyte transdifferentiation model may be more plausible.

To further investigate this transdifferentiation model, we performed genetic lineage tracing of atrial cardiomyocytes in the *Tg*(*vmhc:mCherry–NTR*) ventricle ablation model using an atrial cardiomyocyte specific tamoxifen-inducible Cre transgenic line, *Tg*(*amhc:CreERT2*)^{sd20}, and the indicator transgenic line, *Tg*(*β-actin2:loxP-DsRed-STOP-loxP-eGFP*)^{s928}, hereafter referred to as *β-actin2:RSG* (*β-actin2* is also known as *actb2*), which can effectively label most cells, including cardiomyocytes and endocardial cells, with GFP after tissue-specific Cre-mediated excision of the floxed dsRed cassette[5,13]. Treating the *Tg*(*vmhc:mCherry–NTR*; *amhc:CreERT2*; *β-actin2:RSG*) fish with 4-hydroxytamoxifen (4-HT) at 3 dpf for 4–6 h, effectively GFP labelled all atrial cardiomyocytes by Cre recombination (cre-atrGFP^{+}) without ectopic GFP-labelling of ventricular cardiomyocytes by 5 dpf (Fig. 2c, e; Supplementary Fig. 6a–c); whereas vehicle control treatment resulted in no Cre-mediated GFP labelling of any cells (Supplementary Fig. 6d). We subsequently MTZ-ablated the ventricles of these cre-atrGFP-labelled hearts at 5 dpf (Fig. 2e). In the ablated group, these cre-atrGFP^{+} cardiomyocytes at 96 hpt and at 12 months were present in not only the atrium but also in the ventricle where many of them also co-expressed venCherry ($n = 73/76$; Fig. 2f, Supplementary Figs 7i, j and 8b, c). However, in the control non-ablated group at 96 hpt and at 12 months, cre-atrGFP^{+} cardiomyocytes were only observed in the atrium but never in the ventricle ($n = 0/54$; Fig. 2d; Supplementary Figs 6c and 8a). Using time-lapse imaging within the same ventricle-ablated *Tg*(*vmhc:mCherry–NTR*; *amhc:CreERT2*; *β-actin2:RSG*) hearts, we observed the gradual and contiguous extension of these cre-atrGFP^{+} cardiomyocytes at the AVC into the ventricle where they began to restore ventricular contractile function nearest the AVC and also to exhibit venCherry expression, indicating that they were transdifferentiating from atrial to ventricular cardiomyocytes (Fig. 2g–j, Supplementary Videos 3–5). Electrophysiologic intracellular recordings revealed that these cre-atrGFP^{+} venCherry^{+} cardiomyocytes within the regenerating ventricle exhibited electrical attributes similar to endogenous cre-atrGFP^{-} venCherry^{+} ventricular cardiomyocytes and distinct from atrial cardiomyocytes (that is, cre-atrGFP^{+} venCherry^{-}) (Supplementary Fig. 9). Furthermore, *in situ* analysis showed that the ventricular specific markers *irx1a* and *vmhc* were expressed in ventricular cardiomyocytes at the AVC where cre-atrGFP^{+} ventricular cardiomyocytes reside (Supplementary Fig. 10). Moreover, we also observed that the atrial chamber cre-atrGFP^{+} fluorescence intensity and size in hearts with ablated ventricles appeared to be significantly greater than that of control hearts (compare Fig. 2f to 2d, Supplementary Fig. 7k, l), an observation consistent with the increased atrial size, fluorescence intensity and cardiomyocyte proliferation observed after ventricular injury (Supplementary Figs 2a, b and 4d). Finally, in adult zebrafish ventricles ablated at 4 months, we discovered that the contribution of transdifferentiated atrial cardiomyocytes to the regenerating ventricle was diminished (Supplementary Fig. 11), indicating that this cardiac transdifferentation process may be age-dependent.

To investigate whether these atrial-derived ventricular cardiomyocytes maintained the atrial program, we examined Amhc protein expression by S46 antibody immunostaining in the ventricle-ablated *Tg*(*vmhc:mCherry-NTR*; *amhc:CreERT2*; *β-actin2:RSG*) hearts, and observed that cre-atrGFP^{+} atrial cardiomyocytes continued to express Amhc in the atrium (Fig. 2m, n), but not in the ventricle. However, before their subsequent differentiation into ventricular cardiomyocytes

(cre-atrGFP$^+$ Amhc$^-$ venCherry$^+$ Fig. 2n, Supplementary Fig. 7d, asterisk), we discovered that cre-atrGFP$^+$ cardiomyocytes may first exist in an intermediate dedifferentiation stage (cre-atrGFP$^+$ Amhc$^-$ venCherry$^-$, Fig. 2n, Supplementary Fig. 7d, arrowheads), in which they no longer maintain the atrial program (Amhc$^-$) but have not yet activated the ventricular program (venCherry$^-$). Consistent with these findings, *vmhc* fluorescent *in situ* hybridization also revealed a population of cre-atrGFP$^+$ cardiomyocytes devoid of *vmhc* expression within the recovering ventricle (Fig. 2r, Supplementary Fig. 7h, d arrowheads). Because of this possible dedifferentiation of atrial cardiomyocytes, we also examined the expression of cardiac progenitor markers in the ventricle-ablated hearts. Although we did not detect Isl1 in the injured hearts (data not shown), we did observe the re-expression of *gata4*, *hand2*, *nkx2.5*, *tbx5a* and *tbx20* (Supplementary Fig. 12), as well as increased expression of Mef2 in the atrium, ventricle and outflow tract of the recovering ventricle-ablated hearts (Supplementary Fig. 13). Furthermore, Mef2 immunofluorescence revealed not only that many of the intermediate dedifferentiated cre-atrGFP$^+$ cardiomyocytes within the recovering ventricle (that is, cre-atrGFP$^+$ venCherry$^-$) expressed Mef2 (Supplementary Fig. 13p, arrowheads), but also that the new Mef2$^+$ cells at the outflow tract did not express myosin heavy chain (Supplementary Fig. 13e–h), indicating that these cells may be cardiac progenitor cells, which have not yet differentiated into mature cardiomyocytes. Overall, these data indicate that atrial cardiomyocytes may acquire cardiac progenitor cell attributes to become ventricular cardiomyocytes and moreover that the zebrafish second heart field residing near the outflow tract[14,15] may also contribute ventricular cardiomyocytes to recover the distal portion of the injured ventricle.

To further elucidate the cellular events that take place during ventricular injury and recovery including the atrial-to-ventricular cardiac lineage switch, we analysed the cardiomyocyte structural and morphologic changes after ventricular ablation. To study this, we crossed the *Tg*(*vmhc:mCherry–NTR*) fish to the reporter lines, *Tg*(*cmlc2:actinin–eGFP*)^{sd10} (*cmlc2* is also known as *myl7*) or *Tg*(*cmlc2:eGFP–ras*)^{s883}, which labels sarcomeric structures[16] or outlines cardiomyocytes[17], respectively (Fig. 3a–j, Supplementary Fig. 14), as well as performed N-cadherin immunostaining to examine cardiomyocyte cell–cell junctions (Fig. 3k–o). During ventricular injury, damaged ventricular cardiomyocytes lost their rod-like shape[18], particularly at the outer curvature (Fig. 3g, h, asterisks), and as reported[4,5], exhibited disorganized or complete loss of sarcomeres and cell junctions between 12–24 hpt (Fig. 3b, c, l, m, asterisks), when ventricular function has reached its lowest point. In contrast, during ventricular recovery (36–48 hpt), we observed the reorganization of not only ventricular but also atrial cardiomyocyte sarcomeres, morphologies and adhesion junctions (Fig. 3d, i, n, Supplementary Fig. 14e). In particular, atrial cardiomyocytes at the AVC became more circular (Supplementary Fig. 14b, e) and lost N-cadherin localization at their cell junctions when they began to extend into the ventricle and differentiate into ventricular cardiomyocytes (Fig. 3n). Moreover, we also observed that these migrating atrial cardiomyocytes at the AVC initially displayed disorganized sarcomeric structures (Supplementary Fig. 14d, asterisk), but after populating the ventricle, exhibited enriched actinin-eGFP at the cell periphery/cortex (Fig. 3d, Supplementary Fig. 14d arrow) and frequently short bundles of actinin–eGFP labelled z-line structures (Fig. 3d, Supplementary Fig. 14d, arrowhead), closely resembling *de novo* sarcomere assembly[16]. By 96 hpt when the ventricle has functionally recovered, the ventricular cardiomyocytes derived from reprogrammed atrial cardiomyocytes exhibited not only organized sarcomeres that align with other ventricular cardiomyocytes, but also localization of N-cadherin at the cell junctions (Fig. 3e, o). Overall, these results reveal that atrial cardiomyocytes undergo activated cellular reprogramming following ventricular myocardial injury in order to initiate cellular events that permit their proliferation, migration and transdifferentiation to facilitate ventricular regeneration.

Because previous studies have shown that endocardial activation may be essential to regulate cardiac regeneration[19], we examined Raldh2 (also known as Aldh1a2) expression in ventricle ablated *Tg*(*vmhc:mCherry–NTR*) fish. Although Raldh2 is expressed weakly in control treated hearts (Supplementary Fig. 15a, c, g, h), its expression is induced throughout the endocardium of the ventricle-ablated hearts by 24–48 hpt (Supplementary Fig. 15b, d, k, l). Using the *Tg*(*tp1:eGFP*)^{um14} Notch reporter line[20], we also observed that Notch signalling (that is, *tp1*:eGFP expression) was specifically activated in atrial endocardial cells of *Tg*(*vmhc:mCherry–NTR*) MTZ-ablated hearts, as detected by the overlapping expression between *tp1*:eGFP and *kdrl*:mCherry (*Tg*(*kdrl:ras–mCherry*)^{s896}), which labels endothelial and endocardial cell membranes in red[21] (compare Fig. 4a to b, 4e to f). Whole mount *in situ* hybridization of Notch signalling components revealed that *notch1b* and *deltaD*, which are normally present in the AVC and outflow tract

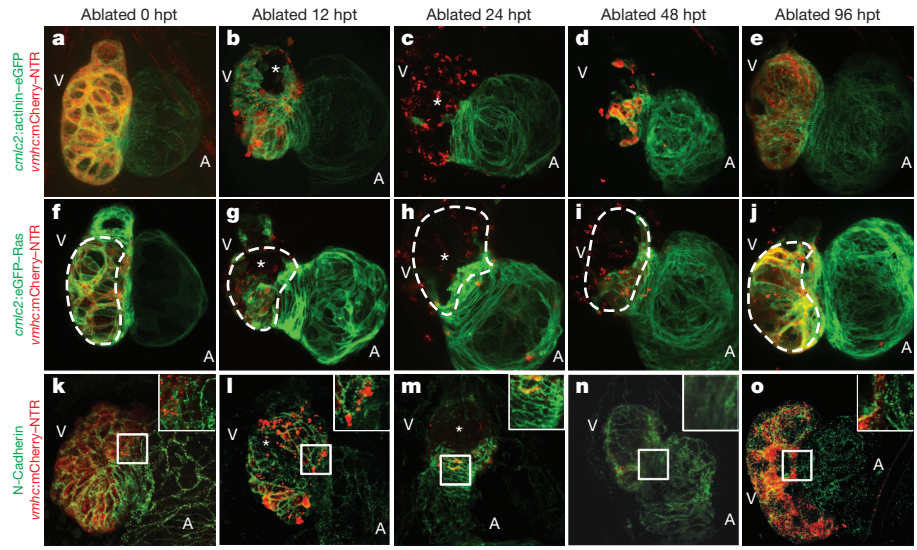

Figure 3 | Dynamic cellular remodelling occurs during zebrafish cardiac regeneration. **a**–**o**, MTZ-treated zebrafish: *Tg*(*vmhc:mCherry–NTR*; *cmlc2:actinin–eGFP*) (**a**–**e**), *Tg*(*vmhc:mCherry–NTR*; *cmlc2:eGFP–ras*) (**f**–**j**), N-cadherin immunostained *Tg*(*vmhc:mCherry–NTR*) (**k**–**o**). 0 hpt (**a**, **f**, **k**); 12 hpt (**b**, **g**, **l**); 24 hpt (**c**, **h**, **m**); 48 hpt (**d**, **i**, **n**) and 96 hpt (**e**, **j**, **o**). Asterisks indicate ventricular cardiomyocyte injury and death due to ablation. Dashed lines indicate the outer curvature ventricular cardiomyocytes. Inset shows the enlargement of the boxed area in **k**–**o** at the AVC. A, atrium; V, ventricle.

of uninjured hearts (Fig. 4i, m), exhibited increased AVC expression as well as activated atrial expression in ventricular-ablated hearts (Fig. 4j, n); however, *deltaC* was absent (Supplementary Fig. 16). Because *tp1*:eGFP expression was strong in the ventricle (Fig. 4a, b), but *notch1b* and *deltaD* expression was not, we performed *gfp* RNA *in situ* analysis to confirm this *tp1*:eGFP ventricular fluorescence and discovered that RNA expression of *gfp* was weak to negligible in both uninjured and injured ventricles (Supplementary Fig. 17a, b), indicating that the relatively robust *tp1*:eGFP ventricular fluorescence may be due to eGFP protein perdurance. Finally, we investigated whether these Notch-activated atrial endocardial cells genetically marked by *Tg*(*kdrl:Cre*)^{s898}; *Tg*(*β-actin2:RSG*)[13] could reprogram into cardiomyocytes to contribute to the regeneration of the ventricle-injured heart, but found no evidence for such an event (data not shown). Conversely, we did not observe any of the genetically marked atrial cardiomyocytes (cre-atrGFP^{+}) becoming endocardial cells (Supplementary Fig. 15i–l).

Thus, to further investigate the importance of this injury-induced atrial Notch activation, we treated ventricle-ablated hearts with the γ-secretase inhibitor, DAPT. As a result, DAPT treatment decreased the ability of these hearts to restore their ventricular morphology and function after injury (control 81%, $n = 96/119$ vs. DAPT-treated 39%, $n = 52/132$; Fig. 4h), which may be due to overall decreased atrial and ventricular cardiomyocyte proliferation (Supplementary Fig. 18). To determine how DAPT impairs this recovery process, we examined the expression of *tp1*:eGFP as well as the migration of genetically labelled atrial cardiomyocytes in DAPT-treated ventricle-injured hearts. We observed not only decreased *tp1*:eGFP expression in the atrium (Fig. 4d), but also a reduction in the migration of cre-atrGFP^{+} atrial cardiomyocytes into the injured ventricle (Fig. 4g). Consistent with these findings, DAPT also inhibited *notch1b*, *deltaD* and *tp1:egfp* expression in the atrium of ventricle-injured hearts (Fig. 4l, p, Supplementary Fig. 17d), but increased *notch1b* and *deltaD* in the outflow tract of uninjured hearts (Fig. 4k, o). Thus, these data indicate that atrial endocardial Notch activation may be crucial to non-cell-autonomously regulate ventricle regeneration through the modulation of atrial-to-ventricular transdifferentiation.

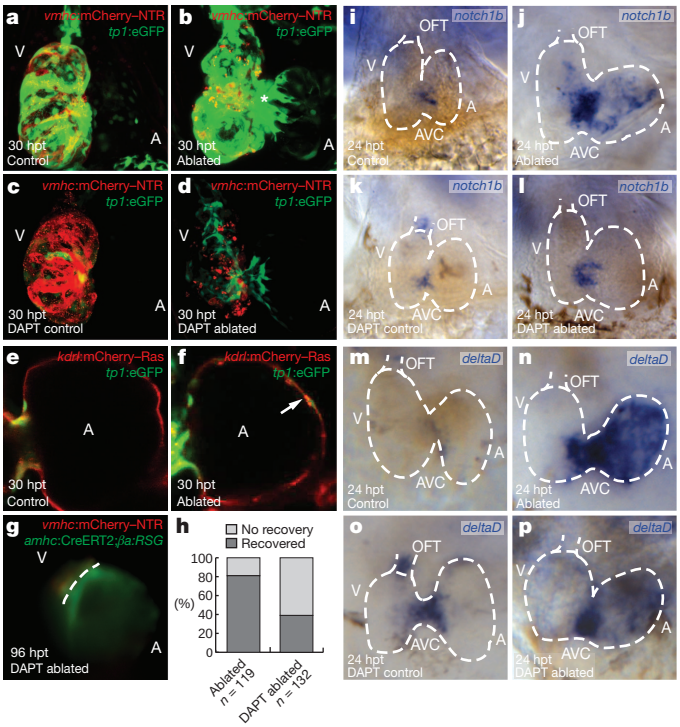

Figure 4 | Notch signalling is required for zebrafish cardiac regeneration. **a**–**d**, 30 hpt *Tg*(*vmhc:mCherry–NTR*; *tp1:eGFP*) control (**a**); ablated (**b**); DAPT-treated control (**c**); DAPT-treated ablated (**d**) hearts. **e**, **f**, Atrium of 30 hpt *Tg*(*vmhc:mCherry-NTR*; *tp1:eGFP*; *kdrl:mCherry*) control (**e**) and ablated (**f**) hearts. Arrow indicates endocardial *tp1*:eGFP expression. **g**, DAPT-treated 96 hpt *Tg*(*vmhc:mCherry-NTR*; *amhc:CreERT2*; *β-actin2:RSG*) ablated ventricles. Dashed line indicates atrioventricular boundary. **h**, Recovery of 96 hpt control and DAPT-treated *Tg*(*vmhc:mCherry–NTR*; *amhc:CreERT2*; *β-actin2:RSG*) ablated fish. **i**–**p**, *notch1b* (**i**–**l**) and *deltaD* (**m**–**p**) *in situ* hybridization on control (**i**, **k**, **m**, **o**) or ablated (**j**, **l**, **n**, **p**) *Tg*(*vmhc:mCherry–NTR*) hearts (dashed lines) at 24 hpt. DAPT-treated (**k**, **l**, **o**, **p**). A, atrium; AVC, atrioventricular canal; OFT, outflow tract; V, ventricle.

Overall, these results reveal that *in vivo* reprogramming of differentiated atrial cardiomyocytes can be induced by cardiac ventricular injury through Notch-mediated signalling and proceeds in distinct intermediate stages (Supplementary Fig. 19) in order to provide a novel endogenous cellular source for cardiac ventricular regeneration in zebrafish. Similar to recent cardiac-injury studies in zebrafish and mouse neonatal hearts, this process may be mediated through the activation of Raldh2 and Notch pathways[19,22], which may lead to sarcomeric reorganization[4,5], cardiomyocyte migration[4,5], and the re-expression of key early cardiac transcriptional regulators such as Gata4, Hand2, Mef2, Nkx2.5, Tbx5, and Tbx20[5,6,23]. Although Raldh2 was expressed throughout the endocardium of the ventricle-injured heart as previously described[6,19], Notch signalling was activated primarily in the atrial endocardium. As a result, we speculate that Notch-activated atrial endocardium may influence the atrial myocardium, just as Notch signalling in the ventricular endocardium influences ventricular trabeculation[24]. Given that previous studies have shown that specific congenital heart diseases can arise from aberrant Notch signalling[25], our studies also raise the possibility that abnormal reprogramming of cardiac lineages may be partially responsible for these heart defects.

Although it remains to be elucidated whether mammalian atrial cardiomyocytes may also have a comparable transdifferentiation capacity, recent studies have indicated that mammalian cardiomyocyte progenitor cells (CPMCs) appear to be enriched in the atrium[26–28] suggesting that the zebrafish transdifferentiating atrial cardiomyocytes may be analogous to the atrial-resident adult CPMCs. Alternatively, mammalian atrial cardiomyocytes could reprogram into ventricular cardiomyocytes through the reactivation of early cardiac transcriptional factors, a process recently reported to reprogram cardiac fibroblasts into ventricular cardiomyocytes in mouse hearts[29,30]. Thus, future studies in mammalian ventricular injury models[6] using similar atrial genetic lineage tracing strategies as presented here, are warranted to further investigate the potential of this cardiac reprogramming process as an endogenous cellular regenerative therapy in human heart failure patients. Such a cardiac regenerative strategy could overcome current obstacles facing the translation of stem-cell therapies for heart failure patients, including the differentiation of autologous cardiac progenitor cells into ventricular cardiomyocytes as well as the delivery and integration of these differentiated ventricular cardiomyocytes into the patient's ventricular myocardium.

METHODS SUMMARY

Chamber-specific ablation and reporter lines were generated using the standard I-*Sce*I meganuclease transgenesis technique (details in Methods). To perform ventricular cardiomyocyte ablation, *Tg*(*vmhc:mCherry–NTR*) zebrafish were treated with 5 mM MTZ as previously described[9]. For lineage tracing experiments, *Tg*(*vmhc:mCherry–NTR*; *amhc:CreERT2*; *β-actin2:RSG*) zebrafish were treated with 10 μM 4-hydroxytamoxifen as previously described[5]. For Notch inhibition studies, zebrafish were treated with 100 μM DAPT. Live imaging, heart contraction, immunofluorescence and whole mount *in situ* hybridization were performed as described in the Methods.

Full Methods and any associated references are available in the online version of the paper.

Received 23 July 2012; accepted 23 May 2013.
Published online 19 June 2013.

1. Bergmann, O. *et al.* Evidence for cardiomyocyte renewal in humans. *Science* **324,** 98–102 (2009).
2. Senyo, S. E. *et al.* Mammalian heart renewal by pre-existing cardiomyocytes. *Nature* **493,** 433–436 (2013).

3. Laflamme, M. A. & Murry, C. E. Heart regeneration. *Nature* **473,** 326–335 (2011).
4. Jopling, C. *et al.* Zebrafish heart regeneration occurs by cardiomyocyte dedifferentiation and proliferation. *Nature* **464,** 606–609 (2010).
5. Kikuchi, K. *et al.* Primary contribution to zebrafish heart regeneration by *gata4*$^{+}$ cardiomyocytes. *Nature* **464,** 601–605 (2010).
6. Porrello, E. R. *et al.* Transient regenerative potential of the neonatal mouse heart. *Science* **331,** 1078–1080 (2011).
7. McDonnell, T. J. & Oberpriller, J. O. The response of the atrium to direct mechanical wounding in the adult heart of the newt, *Notophthalmus viridescens*. An electron-microscopic and autoradiographic study. *Cell Tissue Res.* **235,** 583–592 (1984).
8. Oberpriller, J. O., Oberpriller, J. C. & Aafedt, B. C. Changes in binucleation and cellular dimensions of rat left atrial myocytes after induced left ventricular infarction. *Am. J. Anat.* **179,** 285–290 (1987).
9. Curado, S. *et al.* Conditional targeted cell ablation in zebrafish: a new tool for regeneration studies. *Dev. Dyn.* **236,** 1025–1035 (2007).
10. Zhang, R. & Xu, X. Transient and transgenic analysis of the zebrafish ventricular myosin heavy chain (*vmhc*) promoter: an inhibitory mechanism of ventricle-specific gene expression. *Dev. Dyn.* **238,** 1564–1573 (2009).
11. de Pater, E. *et al.* Distinct phases of cardiomyocyte differentiation regulate growth of the zebrafish heart. *Development* **136,** 1633–1641 (2009).
12. Poss, K. D., Wilson, L. G. & Keating, M. T. Heart regeneration in zebrafish. *Science* **298,** 2188–2190 (2002).
13. Bertrand, J. Y. *et al.* Haematopoietic stem cells derive directly from aortic endothelium during development. *Nature* **464,** 108–111 (2010).
14. Zhou, Y. *et al.* Latent TGF-β binding protein 3 identifies a second heart field in zebrafish. *Nature* **474,** 645–648 (2011).
15. Hinits, Y. *et al.* Zebrafish Mef2ca and Mef2cb are essential for both first and second heart field cardiomyocyte differentiation. *Dev. Biol.* **369,** 199–210 (2012).
16. Lin, Y. F., Swinburne, I. & Yelon, D. Multiple influences of blood flow on cardiomyocyte hypertrophy in the embryonic zebrafish heart. *Dev. Biol.* **362,** 242–253 (2012).
17. D'Amico, L., Scott, I. C., Jungblut, B. & Stainier, D. Y. A mutation in zebrafish *hmgcr1b* reveals a role for isoprenoids in vertebrate heart-tube formation. *Curr. Biol.* **17,** 252–259 (2007).
18. Chi, N. C. *et al.* Genetic and physiologic dissection of the vertebrate cardiac conduction system. *PLoS Biol.* **6,** e109 (2008).
19. Kikuchi, K. *et al.* Retinoic acid production by endocardium and epicardium is an injury response essential for zebrafish heart regeneration. *Dev. Cell* **20,** 397–404 (2011).
20. Parsons, M. J. *et al.* Notch-responsive cells initiate the secondary transition in larval zebrafish pancreas. *Mech. Dev.* **126,** 898–912 (2009).
21. Chi, N. C. *et al.* Foxn4 directly regulates *tbx2b* expression and atrioventricular canal formation. *Genes Dev.* **22,** 734–739 (2008).
22. Raya, A. *et al.* Activation of Notch signaling pathway precedes heart regeneration in zebrafish. *Proc. Natl Acad. Sci. USA* **100** (suppl 1), 11889–11895 (2003).
23. Lepilina, A. *et al.* A dynamic epicardial injury response supports progenitor cell activity during zebrafish heart regeneration. *Cell* **127,** 607–619 (2006).
24. Grego-Bessa, J. *et al.* Notch signaling is essential for ventricular chamber development. *Dev. Cell* **12,** 415–429 (2007).
25. Luxán, G. *et al.* Mutations in the NOTCH pathway regulator *MIB1* cause left ventricular noncompaction cardiomyopathy. *Nature Med.* **19,** 193–201 (2013).
26. Bu, L. *et al.* Human ISL1 heart progenitors generate diverse multipotent cardiovascular cell lineages. *Nature* **460,** 113–117 (2009).
27. Laugwitz, K. L. *et al.* Postnatal isl1^{+} cardioblasts enter fully differentiated cardiomyocyte lineages. *Nature* **433,** 647–653 (2005).
28. Genead, R. *et al.* Early first trimester human embryonic cardiac Islet-1 progenitor cells and cardiomyocytes: Immunohistochemical and electrophysiological characterization. *Stem Cell Res.* **4,** 69–76 (2010).
29. Song, K. *et al.* Heart repair by reprogramming non-myocytes with cardiac transcription factors. *Nature* **485,** 599–604 (2012).
30. Qian, L. *et al. In vivo* reprogramming of murine cardiac fibroblasts into induced cardiomyocytes. *Nature* **485,** 593–598 (2012).

Supplementary Information is available in the online version of the paper.

Acknowledgements We thank N. Tedeschi, L. Pandolfo and A. Ayala for fish care; O. Huang, J. Kim, T. Kuo and J. Sun for experimental assistance; S. Tu and other laboratory members for comments on the manuscript; Q. Liu for anti-N-cadherin antibody; M. Lardelli, J. Lenis and W. Clements for plasmids; and N. Lawson for the Notch reporter line. This work was supported in part by grants from the American Heart Association to D.Y. (0940041N), R.Z. (11POST7090024) and H.Y. (12POST12050080); the Packard Foundation and the National Institutes of Health (NIH) (HL54737) to D.Y.R.S.; NIH/NHLBI (NIH Heart, Lung, and Blood Institute) to J.C.; and the NIH (OD007464, HL104239) to N.C.C.

Author Contributions N.C.C. initiated the project when he was in the laboratory of D.Y.R.S. by generating and validating some of the cardiac chamber specific transgenic lines. Additional experimental design was done with the help of R.Z. and D.Y. R.Z., P.H., Ku.Ou., D.L., G.K. and N.C.C. conducted experiments. R.Z., H.Y. and N.C.C. generated and characterized transgenic lines for lineage tracing. Ka.Oc. and J.C. helped with cardiac function analysis. Y.-F.L. and D.Y. provided key reagents. R.Z., P.H., D.L., D.Y. and N.C.C. prepared the manuscript. All authors commented on the manuscript.

Author Information Reprints and permissions information is available at www.nature.com/reprints. The authors declare no competing financial interests. Readers are welcome to comment on the online version of the paper. Correspondence and requests for materials should be addressed to N.C.C. (nchi@ucsd.edu).

METHODS

Zebrafish husbandry and generation of transgenic fish lines. Zebrafish were raised under standard laboratory conditions at 28 °C. We used the following transgenic lines: *Tg(β-actin2:loxP-DsRed-STOP-loxP-eGFP)*^{s928} *Tg(β-actin2:RSG)*[5], *Tg(cmlc2:actinin–eGFP)*^{sd10} (ref. 16), *Tg(cmlc2:eGFP–ras)*^{s883} (ref. 17), *Tg(tp1:eGFP)*^{um14} (ref. 20) , *Tg (kdrl:ras–mCherry)*^{s896} (ref. 21) and *Tg(kdrl:Cre)*^{s898} (ref. 13). The *Tg(tp1:eGFP)*^{um14} Notch reporter line used for these studies was previously confirmed for reporting Notch activity in the heart as well as other tissues using the mindbomb mutant[25,31,32]. The construct to create *Tg(vmhc:mCherry–NTR)*^{s957} was generated by cloning a 2 kilobase (kb) *vmhc* promoter[10] into the pBSKi vector[33], and the mCherry–nitroreductase fusion gene was then cloned downstream of the *vmhc* promoter. The construct used to create *Tg(amhc:eGFP)*^{s958} was generated by cloning a 982 base pair (bp) *amhc* promoter (forward primer: 5′-GCTAAAGTGGCAGTGTGCCG-′3 and reverse primer: 5′-CGTGAATATGGTTTTCAGGAG-′3) into the pBSKi vector, and GFP was cloned downstream of the *amhc* promoter. The construct to create *Tg(amhc:CreERT2)*^{sd20} was generated by cloning a 4.5 kb *amhc* promoter (forward primer: 5′-CCTGGAACTCAACAATGCTC-′3 and reverse primer: 5′-GATCT GGATCTCTCCTCAGTTG-′3) into the pBSKi vector, and CreERT2[34] was cloned downstream of the *amhc* promoter. We injected 200 pg of each linearized DNA into one-cell-stage embryos and selected individual transgenic carrier adults by screening for fluorescent progeny.

MTZ treatment. *Tg(vmhc:mCherry–NTR)* larval and adult zebrafish were treated with 5 or 10 mM MTZ in egg or zebrafish system water for four hours and two days, respectively, at 28 °C in the dark as previously described[35]. As controls, age-matched *Tg(vmhc:mCherry–NTR)* siblings were incubated in 0.2% DMSO (dimethylsulphoxide) in egg or zebrafish system water. Treated zebrafish were washed with several changes of fresh egg or zebrafish system water at the end of ablation and then allowed to continue to grow in fresh egg or zebrafish system water.

TUNEL. Using the *in situ* cell death detection kit, fluorescein from Roche (11684795910), fish hearts were examined for cell death by TUNEL staining. Specifically, zebrafish at the indicated stages were fixed with 4% paraformaldehyde (PFA), permeabilized with PBS with 0.5% TritonX-100 and then incubated in TUNEL staining solution at 37 °C for 2 h.

Immunofluorescence. Immunofluorescence staining was performed as previously described[36]. The primary antibodies used in this study include: anti-GFP (chicken; Aves Labs); anti-Isl (ref. 11) (mouse; Developmental Studies Hybridoma Bank); anti-Mef2/C-21 (ref. 15) (rabbit; Santa Cruz Biotechnology); MF20/anti-MHC (ref. 37) (mouse; Developmental Studies Hybridoma Bank); anti-N-cadherin (ref. 38) (rabbit; courtesy of Q. Liu); anti-phospho-histone H3 (rabbit; Upstate), anti-Raldh2 (ref. 19) (rabbit; Abmart); and anti-Amhc (S46) (ref. 37) (mouse; Developmental Studies Hybridoma Bank). For the *vmhc* fluorescent *in situ* hybridization studies, GFP antibody was used to detect the GFP genetically labelled atrial cardiomyocytes. Raldh2 antibody was used to examine endocardial and epicardial activation during cardiac injury[19]. The secondary antibodies used in this study include: Alexa Fluor 488 goat anti-mouse IgG, Alexa Fluor 488 goat anti-rabbit IgG, Alexa Fluor 594 goat anti-mouse IgG, Alexa Fluor 633 goat anti-mouse IgG, Alexa Fluor 647 goat anti-rabbit IgG from Invitrogen and anti-chicken IgY-FITC from Sigma. Fluorescent images were obtained using a Leica SP5 or Nikon C2 confocal microscope.

***in situ* hybridization.** Whole mount *in situ* hybridization was performed as previously described[18], using the following probes: *amhc*, *deltaC* (courtesy of J. Lenis), *deltaD* (courtesy of W. Clements), *gata4*, *gfp*, *hand2*, *irx1a*, *nkx2.5*, *notch1b* (courtesy of M. Lardelli), *tbx5a, tbx20* and *vmhc*. *vmhc* fluorescent *in situ* hybridization[37] was performed as previously described[39] using single digoxygenin-labelled riboprobe and detected by TSA Plus Cy5 Solution (Perkin Elmer).

Cardiac contractile analysis. Live zebrafish were embedded in 1% low melting agarose in a glass bottom culture dish (MatTek), and the heart contraction was recorded by a high speed EMCCD camera (Hamamatsu). The heart function was analysed as previously described[40]. The fractional area change was calculated as FC = (End diastolic area − End systolic area)/End diastolic area × 100%.

Intracellular action potential recording. Adult zebrafish hearts were mounted in a chamber containing Tyrode's solution of the following composition (mM): NaCl 150, KCl 5.4, $MgSO_4$ 1.5, NaH_2PO_4 0.4, $CaCl_2$ 2, Glucose 10, HEPES 10. The pH of the solution was adjusted to pH 7.4 with NaOH. Glass pipettes with tip resistance 30–40 MΩ were filled with 3M KCl solutions. The hearts were allowed to equilibrate for 10 min before spontaneous intracellular action potentials were recorded using an Axopatch 200B amplifier and pClamp10.3 software (Molecular Devices, LLC). Electrophysiologic intracellular recordings were performed on transdifferentiated ventricular cardiomyocytes (cre-atrGFP$^+$ venCherry$^+$), endogenous ventricular cardiomyocytes (cre-atrGFP$^-$ venCherry$^+$) and atrial cardiomyocytes (cre-atrGFP$^+$ venCherry$^-$). All experiments were performed at room temperature (20–22 °C). $n = 5$ hearts.

Tamoxifen treatment and lineage tracing. *Tg(vmhc:mCherry–NTR; amhc:CreERT2; β-actin2:RSG)* zebrafish were treated with 10 μM 4-hydroxytamoxifen (4-HT) solution (Sigma) or 0.1% ethanol alone (control) at 72 hpf for 6 h at 28 °C and then washed with fresh egg water several times. The ventricles of hearts with GFP genetically labelled atrial cardiomyocytes were then ablated at 96–120 hpf ($n = 76$) or at 4 months ($n = 23$). Live zebrafish were embedded in 0.5% low melting agarose in a glass bottom culture dish as previously described[41] for time-lapse imaging using a Leica M205FA stereomicroscope with a DFC310FX camera. The hearts were then collected at indicated time points post treatment, cryosectioned and examined under a Nikon C2 confocal microscope.

Cryosection and histology staining. Adult zebrafish hearts were fixed in 4% PFA for 2 h at room temperature and equilibrated through 15% and then 30% sucrose in PBS for several hours until they sank down to the bottom. Hearts were embedded in O.C.T. compound (Tissue-Tek, 4583) and frozen in liquid nitrogen. 10-μm cryosections were prepared on a Leica CM3050 S cryostat. Masson's trichrome staining was performed using the Sigma HT15 kit.

DAPT treatment. Zebrafish were incubated in egg water with 100 μM DAPT (Sigma) or 0.1% DMSO alone (control) right after ablation until the zebrafish were fixed or examined at indicated stages. Treated zebrafish were washed several times in egg water after DAPT or DMSO treatment.

Quantification and statistical analysis. To measure cardiac chamber size, *Tg(vmhc:mCherry–NTR)* hearts were visualized by bright field microscopy at the indicated conditions, and the cardiac chamber size was calculated by measuring the surface area of outlined chambers using Leica LAS AF software ($n = 10$). To determine average fluorescence intensity for each chamber, *Tg(vmhc:mCherry–NTR; cmlc2:actinin–eGFP)* hearts were visualized by confocal microscopy at the indicated stages, and average fluorescence intensity was calculated by measuring the fluorescence intensity of outlined maximal projections of cardiac chambers using Nikon NIS Elements software ($n = 5$). Cardiomyocyte surface area and circularity were measured by outlining single cardiomyocytes on confocal maximal projection images of *Tg(vmhc:mCherry–NTR; cmlc2:eGFP–ras)* hearts using the Nikon NIS Elements software ($n = 15$, 5 cells per heart, 3 hearts) as previously described[18]. Circularity was calculated as circularity $= 4 \times \pi$ area/perimeters^2. To determine the percentage of the *Tg(vmhc:mCherry–NTR; amhc:CreERT2; β-actin2:RSG)* ventricles that was GFP positive, the measured GFP positive surface area of the cardiac ventricles as detected by confocal microscopy was divided by the measured total surface area of the cardiac ventricles as detected by brightfield microscopy. To determine the surface area and average fluorescence intensity of the *Tg(vmhc:mCherry–NTR; amhc:CreERT2; β-actin2:RSG)* atria, the atrial chamber surface area and fluorescence were measured in the bright field and GFP channel using the Nikon NIS Elements software ($n = 5$). *P* values were obtained by unpaired two-tailed Student's *t*-test.

31. Ninov, N., Borius, M. & Stainier, D. Y. Different levels of Notch signaling regulate quiescence, renewal and differentiation in pancreatic endocrine progenitors. *Development* **139,** 1557–1567 (2012).
32. Wang, Y., Rovira, M., Yusuff, S. & Parsons, M. J. Genetic inducible fate mapping in larval zebrafish reveals origins of adult insulin-producing β-cells. *Development* **138,** 609–617 (2011).
33. Thermes, V. *et al.* I-SceI meganuclease mediates highly efficient transgenesis in fish. *Mech. Dev.* **118,** 91–98 (2002).
34. Feil, R. *et al.* Ligand-activated site-specific recombination in mice. *Proc. Natl Acad. Sci. USA* **93,** 10887–10890 (1996).
35. Curado, S., Stainier, D. Y. & Anderson, R. M. Nitroreductase-mediated cell/tissue ablation in zebrafish: a spatially and temporally controlled ablation method with applications in developmental and regeneration studies. *Nature Protocols* **3,** 948–954 (2008).
36. Huang, W., Zhang, R. & Xu, X. Myofibrillogenesis in the developing zebrafish heart: A functional study of tnnt2. *Dev. Biol.* **331,** 237–249 (2009).
37. Stainier, D. Y. & Fishman, M. C. Patterning the zebrafish heart tube: acquisition of anteroposterior polarity. *Dev. Biol.* **153,** 91–101 (1992).
38. Kerstetter, A. E., Azodi, E., Marrs, J. A. & Liu, Q. Cadherin-2 function in the cranial ganglia and lateral line system of developing zebrafish. *Dev. Dyn.* **230,** 137–143 (2004).
39. Brend, T. & Holley, S. A. Zebrafish whole mount high-resolution double fluorescent *in situ* hybridization. *J. Vis. Exp.* http://dx.doi.org/10.3791/1229 (2009).
40. Fink, M. *et al.* A new method for detection and quantification of heartbeat parameters in Drosophila, zebrafish, and embryonic mouse hearts. *Biotechniques* **46,** 101–113 (2009).
41. Dong, Z., Wagle, M. & Guo, S. Time-lapse live imaging of clonally related neural progenitor cells in the developing zebrafish forebrain. *J. Vis. Exp.* http://dx.doi.org/10.3791/2594 (2011).